

Optimal Integral Force Feedback and Structured PI Tracking Control: Application for High Speed Confocal Microscopy.

Yik R. Teo* Douglas Russell** Sumeet S. Aphale**
Andrew J. Fleming*

* Precision Mechatronics Lab, School of Electrical Engineering and
Computer Science, The University of Newcastle, Callaghan, N.S.W
2308, Australia (e-mail: yik.teo, andrew.fleming@newcastle.edu.au).

** School of Engineering, University of Aberdeen, United Kingdom

Abstract: In this paper, an improvement to Integral Force Feedback (IFF) damping control is proposed. The main limitation of Integral Force Feedback is that the maximum modal damping depends on the system's parameters. Hence, for some system achievable damping is insignificant. The proposed improvement allows any arbitrary damping ratio to be achieved for a system by introducing a new feed-through term in the system. To achieve displacement tracking, one technique is to enclose the system in an integral feedback loop. However, the bandwidth is limited due to the effects of an additional pole in the damping loop. The proposed Structured PI controller is parameterised so that it contains a zero that cancel the additional pole. Experiment was conducted on a commercial objective lens positioner. The results show an exceptional tracking and damping performance and the system's insensitivity to changes in resonance frequency. The maximum bandwidth achievable with a commercial PID controller is 26.1 Hz. In contrast, with the proposed method, the bandwidth is increased to 255 Hz.

Keywords: Force Feedback, Damping Control, Nanopositioning

1. INTRODUCTION

High-speed precision positioner are widely used in application such as confocal microscopes [Semwogerere and Weeks, 2005], scanning probe microscopy [Salapaka and Salapaka, 2008, Fleming and Leang, 2014] and electrical characterization of semiconductor [Oliver, 2008]. In this paper, we are interested in improving the scanning performance of a objective lens positioner used in confocal microscopes. The objective lens positioner can be represented by a single-degree-of-freedom mechanical system as shown in Fig. 1. One difficulty with the positioning system shown in Fig. 1 is the mechanical resonances that appears from the interaction between the platform mass with the flexures, mechanical linkages and actuators. Consequently, the frequency of the driving signal for example a triangular reference is limited to to 1% – 10% of the resonance frequency to avoid excitation of the mechanical resonance.

Sensor-based feedback control using proportional-integral or integral controllers are widely used in commercial nanopositioning systems. The benefits of these controller include robustness to modelling error, simplicity of implementation and reduced piezoelectric non-linearity due to a high loop gain at low frequency. The closed-loop bandwidth of an integral tracking controller $C_t(s) = K/s$ is limited by the presence of highly resonance modes. The maximum closed-loop bandwidth is $2\zeta\omega_n$, where ζ is the damping ratio and ω_n is the natural frequency see Fleming

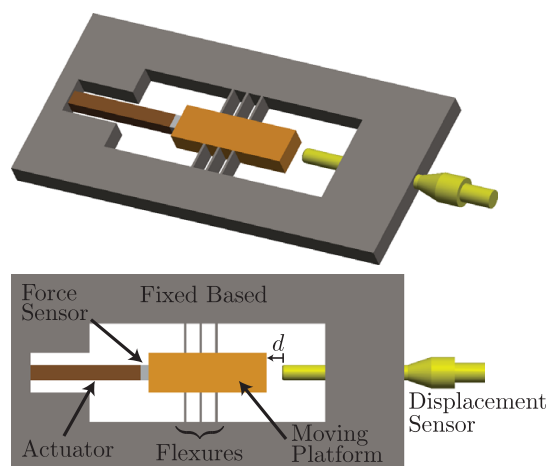


Fig. 1. Single-degree-of-freedom positioning stage.

[2010] and Eilsen et al. [2011]. Since the damping ratio is usually in the order of 0.01, the maximum closed-loop bandwidth is less than 2% of the resonance frequency.

In order to improve the closed-loop bandwidth of nanopositioning system, techniques such as notch filters or plant inversion filters can be implemented [Abramovitch et al., 2008]. Such techniques can provide superior improvement provided an extremely accurate model of the system is available. However, due to the dependency on model accuracy, any small changes in the system dynamics can

result in instability. Notch or plant inversion filters are only practical when the systems with stable resonance frequency or cases when the feedback controller can be continually recalibrated.

Damping control is an alternative method to improve the closed-loop bandwidth. Damping controllers are insensitive to variations in resonance frequency. Furthermore, damping controllers provide better external disturbance rejection than inversion-based systems, see Devasia et al. [2007]. A number of techniques for damping control have been successfully demonstrated in the literature, such as, Positive Position Feedback (PPF) [Fanson and Caughey, 1990], polynomial based control [Aphale et al., 2008], acceleration feedback [Mahmoodi and Ahmadian, 2010], shunt control [Fleming and Moheimani, 2006, Fleming et al., 2002], resonant control [Pota et al., 1999], and Integral Resonance Control (IRC) [Aphale et al., 2007, Fleming et al., 2010].

Integral force feedback (IFF) a damping control technique described in references Preumont et al. [1992, 2008], Preumont [2002, 2006], Fleming [2010], Fleming and Leang [2010]. The advantages of IFF are the simplicity of the controller, guaranteed stability and excellent performance robustness. Furthermore, IFF can also be implemented using an analog filter. However, one of the limitations of IFF is that the maximum modal damping depends on the frequency difference between the system's poles and zeros. If the frequency difference is small, the achievable modal damping may be severely limited. Furthermore, when the IFF system is enclosed in a tracking loop, the closed-loop performance is limited by an additional pole introduced by the integral force feedback controller.

In this paper, we proposed a technique that allows an arbitrary damping ratio to be achieved by introducing an additional feed-through term to the control system. This allows the position of the zeros to be modified, hence, increasing the maximum modal damping. Furthermore, we identified the additional pole that is introduced by the force feedback controller and compensate it by parameterising the tracking controller with a zero that cancels the additional pole.

The remainder of the paper is organised as follows. In Section 2, the modelling of a single-degree-of-freedom positioning system is shown. Section 3 compares the proposed damping control technique with classical integral force feedback control. The tracking controller designs are discussed in Section 4. The experimental result on a commercial objective lens positioner in Section 5.

2. MODELLING A NANOPositionING SYSTEMS

A single-degree of freedom positioner illustrated in Fig. 1 can be represented by a second-order mechanical system as shown in Fig. 2. The equation of motion for this system is

$$M_p \ddot{d} + c_f \dot{d} + (K_a + k_f)d = F_a, \quad (1)$$

where M_p is the mass of the platform and the stiffness and damping coefficient of the flexures are denoted by k_f and c_f respectively. The force of the actuator is F_a and the stiffness is K_a . A force sensor is collocated with the actuator and measures the load force F_s . The configuration

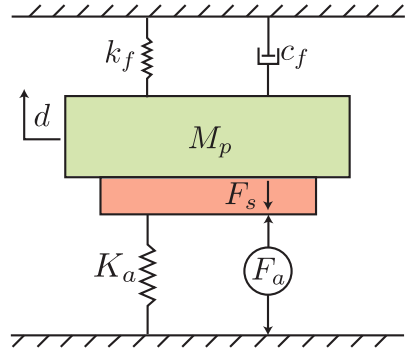


Fig. 2. Mechanical diagram of a single-degree-of freedom positioner where F_s is the measured force acting between the actuator and the mass of the platform in the vertical direction.

of the system is such that the actuator and flexure appear mechanically in parallel, hence, the stiffness coefficients can be grouped together, $k = K_a + k_f$, which simplifies the equation of motion (1) to

$$M_p \ddot{d} + c_f \dot{d} + k = F_a. \quad (2)$$

The transfer function from actuator force F_a to the displacement of the platform d is

$$G_{dF_a}(s) = \frac{d}{F_a} = \frac{1}{M_p s^2 + c_f s + k}.$$

The sensor force F_s can be written as

$$F_s = F_a - dK_a = F_a (1 - K_a G_{dF_a}). \quad (3)$$

The transfer function between the applied force F_a and measured force F_s is found by rearranging (3).

$$G_{F_s F_a}(s) = \frac{F_s}{F_a} = 1 - K_a G_{dF_a}(s). \quad (4)$$

The force developed by the actuator F_a is

$$F_a = K_a \delta \quad (5)$$

where δ is the unconstrained piezo expansion. Substituting (5) into (4), we obtain the transfer function from the unconstrained piezo expansion δ to the force of the sensor F_s

$$G_{F_s \delta}(s) = \frac{F_s}{\delta} = K_a \frac{F_s}{F_a} = K_a (1 - K_a G_{dF_a}). \quad (6)$$

A valid assumption is that the effect of the damping in the flexure c_f is small and thus negligible. The frequencies of the open-loop poles ω_1 and zeros z_1 of (4) are

$$\omega_1 = \sqrt{\frac{k}{M_p}} = \sqrt{\frac{K_a + k_f}{M_p}}, \quad z_1 = \sqrt{\frac{k_f}{M_p}}. \quad (7)$$

The zeros will appear below the poles as shown in Fig. 3.

3. DAMPING CONTROL

Integral force feedback (IFF) is a popular method for damping control, as described in references Preumont et al. [2008], Preumont [2006], Fleming [2010], Fleming and Leang [2010]. This technique utilizes a force sensor and integral controller to directly augment the damping of a mechanical system. The major advantages of IFF are the simplicity of the controller, guaranteed stability, excellent performance robustness, and the ability to damp a large number of resonance modes with a first order controller.

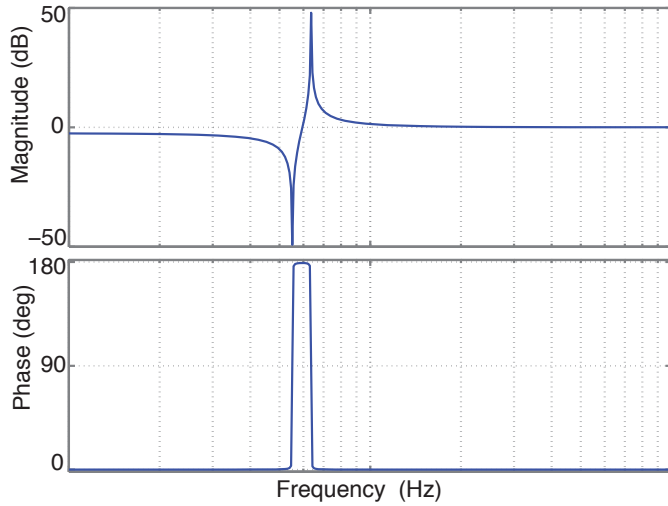


Fig. 3. Typical frequency response of $G_{F_s F_a}(s)$.

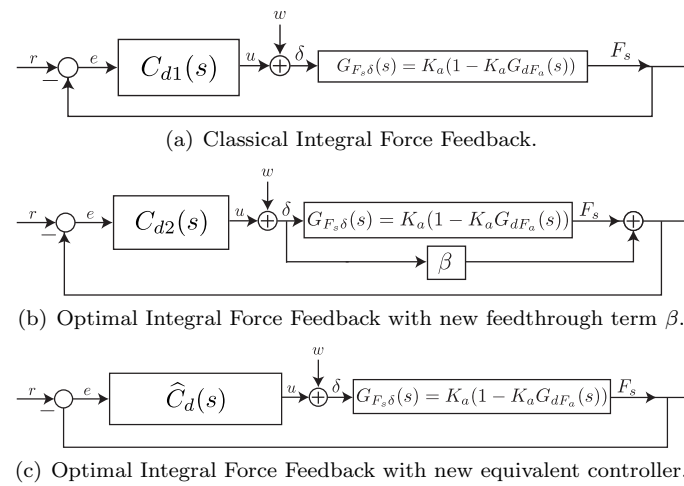


Fig. 4. Damping control block diagrams

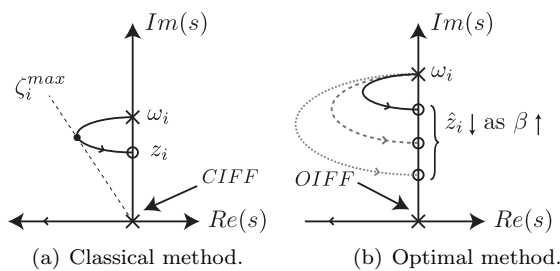


Fig. 5. Typical root-locus plots.

3.1 Classical Integral Force Feedback

The technique of Classical Integral Force Feedback (CIFF) has been widely applied for augmenting the damping of flexible structures. The feedback law is simple to implement and, under common circumstances, provides excellent damping performance with guaranteed stability.

The open loop transfer function between the unconstrained piezo expansion δ to the sensor force F_s is adapted from Preumont et al. [2008]

$$G_{F_s \delta}(s) = \frac{F_s}{\delta} = K_a \left\{ 1 - \sum_{i=1}^n \frac{v_i}{1 + s^2/\omega_i^2} \right\}, \quad (8)$$

where the sum extends to all the modes, ω_i is the natural frequency of the system and v_i is the fraction of modal strain energy for the i^{th} mode. The corresponding zeros of each mode is given as $z_i^2 = \omega_i^2(1 - v_i)$.

For the positioning application the first resonance mode is of significant interest, this reduce (8) to a second order system (6). The feedback diagram of an IFF damping controller is shown in Fig. 4(a). The frequency response of $G_{F_s F_a}$ is shown in Fig. 3. A key observation of the system $G_{F_s F_a}$ is that its phase response lies between 0 and 180°. This is a general feature of flexible structures with inputs and outputs proportional to applied and measured forces. A unique property of such systems is that integral control can be directly applied to achieve damping, i.e.

$$C_{d1}(s) = \frac{K_{d1}}{K_a s}, \quad (9)$$

where K_{d1} is the damping control gain. As the integral controller has a constant phase lag of 90°, the loop-gain phase lies between -90 and 90°. That is, the closed-loop system has an infinite gain margin and phase margin of 90°. Simplicity and robustness are two outstanding properties of systems with CIFF.

A solution for the optimal feedback gain K_d has already been derived in Preumont et al. [2008]. These results can be directly adapted for the system considered in this study. The method makes the valid assumption that system damping coefficients are small and can be neglected. With these assumptions, the maximum modal damping is Preumont et al. [2008]

$$\zeta_i^{max} = \frac{\omega_i - z_i}{2z_i}, \quad (10)$$

and is achieved for

$$K_{d1} = \omega_i \sqrt{\omega_i/z_i}. \quad (11)$$

The root locus plot corresponding to CIFF is shown in Fig. 5(a). Note that a key characteristic of this system is that the position of the poles and zeros alternates. The main limitation of the classical method is that the maximum modal damping (10) depends on the distance between the system poles ω_i and modal zeros z_i . If the distance between the pole and zero is small, the maximum modal damping achievable with CIFF is reduced.

3.2 Optimal Integral Force Feedback (OIFF)

Here, we discuss an extension to the classical technique of Integral Force Feedback that allows an arbitrary damping ratio to be achieved for any system. A new feed-through term β is introduced into the system as shown in Fig. 4(b). The location of the new open-loop zeros is given as

$$\hat{z}_i(\beta) = \sqrt{\omega_i^2 \left(1 - \frac{K_a}{K_a + \beta} \frac{K_a}{k} \right)}. \quad (12)$$

This results in an extra degree of freedom that allows the position of the zeros to be modified. As β decreases, the zeros of the system will move closer to the real axis, under the condition that $K_a(v_i - 1) < \beta < 0$ is satisfied. The new maximum damping ratio of the system is given as

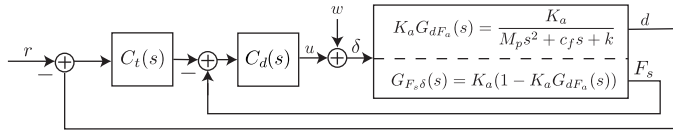


Fig. 6. Block diagram of the overall system including inner damping loop and the outer tracking loop.

$$\hat{\zeta}_i^{max} = \frac{\omega_i - \hat{z}_i(\beta)}{2\hat{z}_i(\beta)}, \quad (13)$$

The force feedback control is

$$C_{d2}(s) = \frac{K_{d2}}{(K_a + \beta)s} \quad (14)$$

The corresponding optimal gain is given as

$$K_{d2} = \omega_i \sqrt{\omega_i / \hat{z}_i(\beta)}. \quad (15)$$

Given a desired damping ratio $\zeta_d < 1$, the expression for β is found by replacing (12) into (13) and rearranging the equation as

$$\beta = -K_a + \frac{K_a v_i (2\zeta_d + 1)^2}{4\zeta_d (1 + \zeta_d)}. \quad (16)$$

where $v_i = K_a/k$ for the nanopositioning system in Section 2.

The typical root locus plot corresponding to OIFF is given in Fig. 5(b). Note that the zero location changes with respect to β . The equivalent controller $\hat{C}_d(s)$ can be written as

$$\hat{C}_d(s) = \frac{C_{d2}(s)}{1 + C_{d2}(s)\beta}, \quad (17)$$

as shown in Fig. 4(c). The modification amounts to replacing the integral controller with a first-order low-pass filter. Although the additional complexity is negligible, the damping performance is significantly improved. This result allows integral force feedback control to be applied to systems that were not previously suited.

4. TRACKING CONTROL

4.1 Integral Control with Displacement Feedback

The most straightforward technique for achieving displacement tracking is to simply enclose the system in an integral feedback loop, as depicted in Fig. 6. The tracking controller is

$$C_{t1}(s) = \frac{K_{t1}}{s}. \quad (18)$$

This strategy requires the displacement d and is obtained with a physical sensor i.e. capacitive sensor. However, the damped system contains a pair of resonance poles, plus an additional real axis pole due to OIFF. The additional pole unnecessarily increase the system order and reduces the achievable tracking bandwidth due to low-phase margin.

4.2 Structured PI Control with Displacement Feedback

The location of the additional pole can be found by examining the characteristic equation of the damped system and finding the roots using Cardano's method, see Press et al. [2007]. The roots of the system under consideration



Fig. 7. Queensgate OSM-Z-100B objective lens positioner (Left) and Olympus 4×, 40× and 100× objective lens (Right).

contains a complex pair and a pole on the real axis. To eliminate the additional pole from the tracking loop, the controller can be parameterised so that it contains a zero at the same frequency, that is

$$C_{t2}(s) = \frac{K_{t2}(s+p)}{sp}, \quad (19)$$

where p is the location of the additional pole given as

$$p = -(A + B - a/3),$$

$$a = K_{d2} + \frac{c_f}{M_p},$$

$$b = \frac{k + c_f K_{d2}}{M_p},$$

$$c = \frac{K_{d2}(-K_a^2 + k(K_a + \beta))}{M_p(K_a + \beta)},$$

$$Q = \frac{a^2 - 3b}{9}, \quad R = \frac{2a^3 - 9ab + 27c}{54},$$

$$A = -\sqrt[3]{R + \sqrt{R^2 - Q^3}}, \quad B = Q/A.$$

The integral gain is chosen in the normal way to provide the desired stability margins. The form of this controller is identical to a PI controller except that the zero location is fixed. This is advantageous since the controller has only one free tuning parameter.

5. EXPERIMENTAL RESULTS

The experiment was conducted on a Queensgate OSM-Z-100B objective lens positioner with 3 different lens as shown in Fig. 7. This single-axis positioner has a range of 100 μm and a static stiffness of 1.5 $\text{N}/\mu\text{m}$. The weight of the objective lens are given in Table 1. The inner loop damping controller is implemented using analog electronics. The outer tracking loop is implemented using a Queensgate NPS4110 controller. The block diagram of the experimental set-up is shown in Fig. 8.

By referring to the set-up in Fig. 8, the open-loop frequency response shown in Fig. 9 was measured from the voltage amplifier input u_2 to the force sensor F_s and position sensor output d with an excitation of 100 mV_{pp} random noise signal. The voltage amplifier input is proportional to the internal force of the actuator F_a . The open-loop frequency responses are shown in Fig. 10 which reveal an extremely high modal density. The first two modes are relative close in frequency. This open loop system with

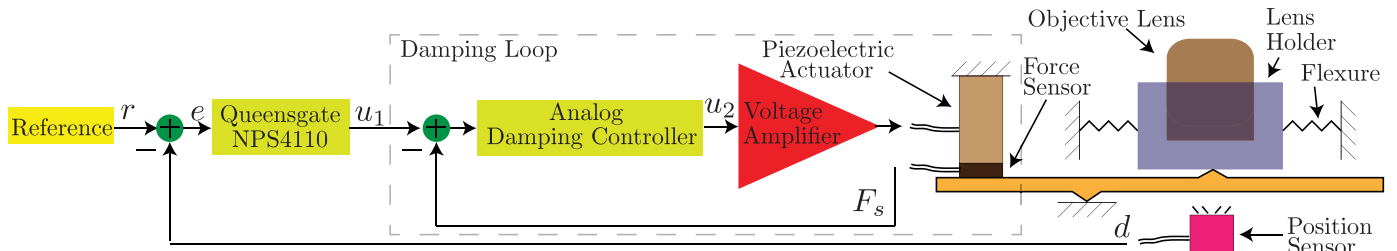


Fig. 8. Block diagram of the experimental setup.

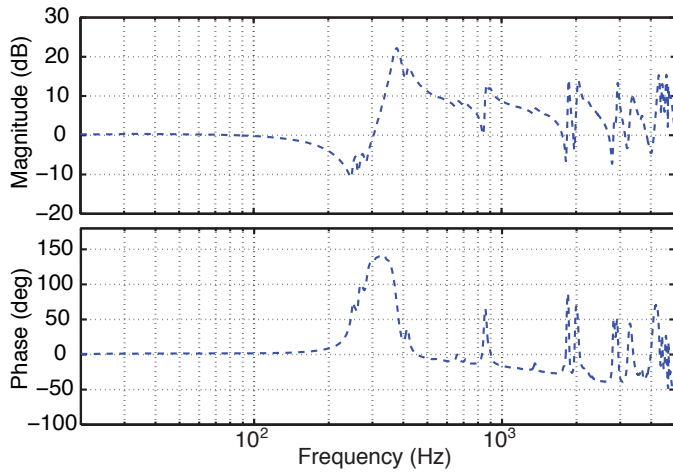


Fig. 9. Open-loop frequency response measured from the voltage amplifier input u_2 to the force sensor F_s .

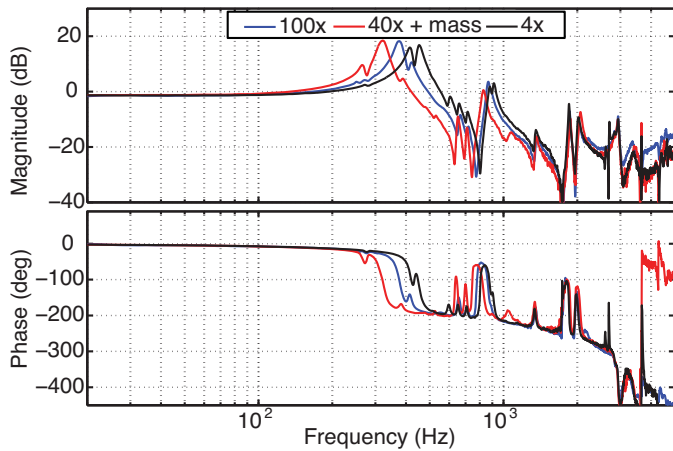


Fig. 10. Open-loop frequency response measured from voltage amplifier input u_2 to position sensor output d , scaled to $\mu\text{m}/\text{V}$ for different objectives.

the 100 \times objective lens attached can be approximated by a second-order transfer function

$$G_{F_s F_a}(s) = \frac{2.141s^2 + 736.4s + 6.072 \times 10^6}{s^2 + 214s + 5.606 \times 10^6} \quad (20)$$

5.1 Damping Control

The maximum damping ratio and corresponding gain of the system with CIFF is $K_{d1} = 1500$ and $\zeta_1^{max} = 0.3$. The numerically found values are $K_{d1} = 1700$ and $\zeta_1^{max} = 0.33$ obtained from the root locus plot in Fig. 12. With OIFF,

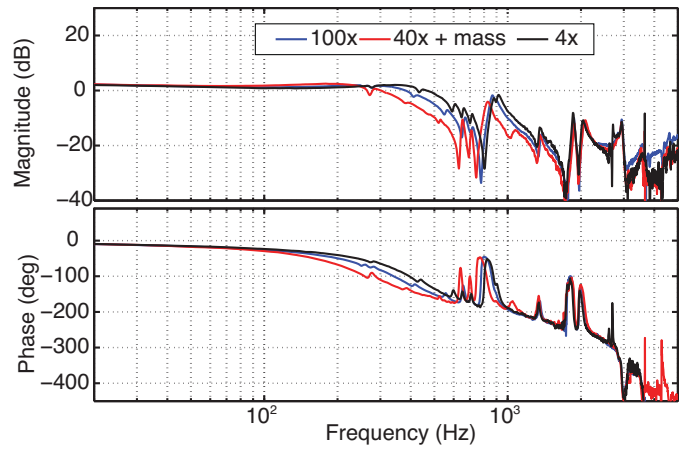


Fig. 11. Closed-loop frequency response of the inner damping loop measured from u_2 to the position sensor output d , scaled to $\mu\text{m}/\text{V}$ for different objectives.

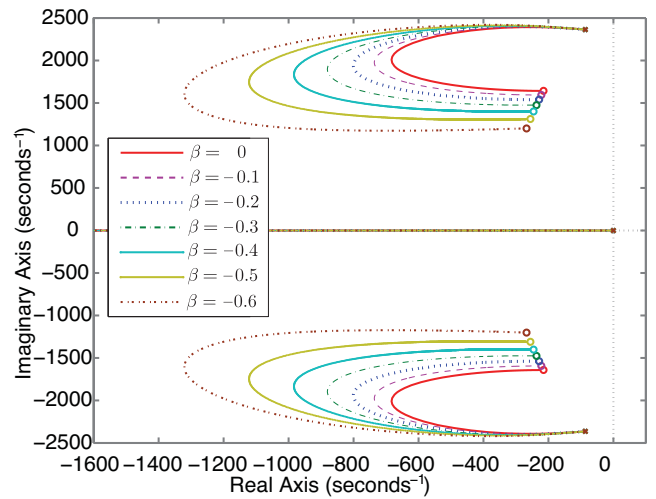


Fig. 12. Root-locus of the system using OIFF.

the damping ratio can be increased from 0.33 to 0.85 by adjusting the value of the feed-through term β . Fig. 12 shows the root locus plots of the system using OIFF with different value of β and Fig. 13 shows the relationship between β and ζ .

Fig. 11 also shows the closed-loop frequency responses of the inner damping loop of the system using OIFF with $\beta = -0.6$. The closed-loop frequency responses are measured using the same procedure as the open-loop responses. The closed-loop response shows that the first resonance modes have been effectively damped. Moreover, it can be observed

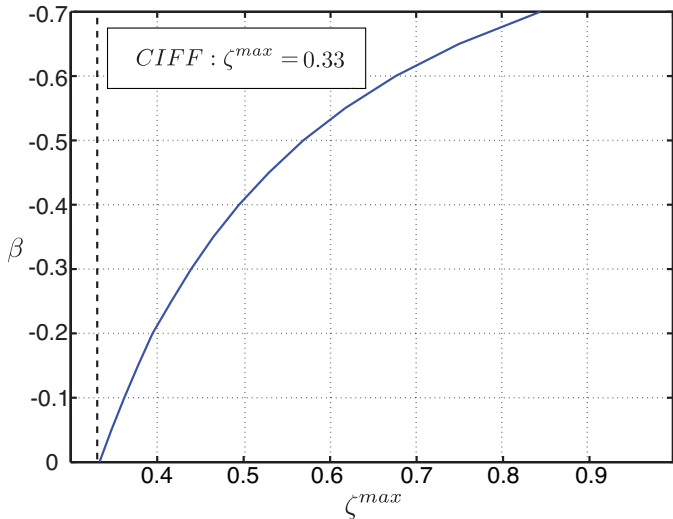
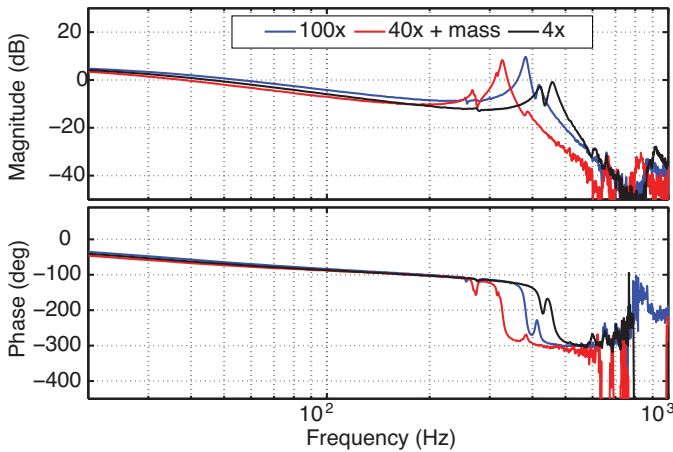
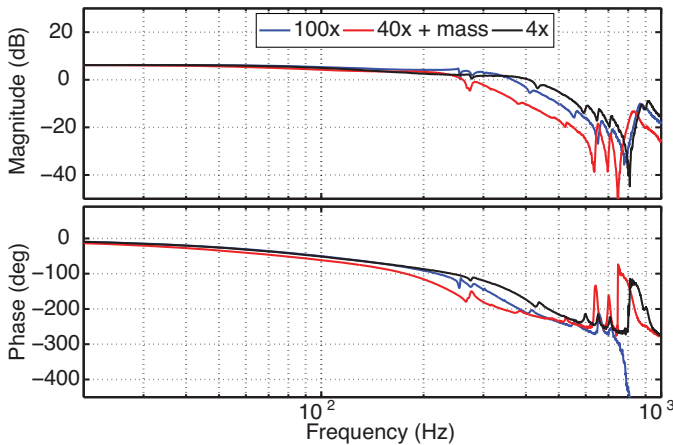


Fig. 13. The relationship between ζ^{max} and β using OIFF.



(a) Commercial PID controller.



(b) OIFF + Structured PI control.

Fig. 14. Closed-loop frequency responses of the system measured from the reference r to the output of the position sensor d scaled to $\mu\text{m}/\text{V}$ for different objectives.

that for other objectives the tuning of the force-feedback loop is not sensitive to changes in resonance frequency.

Table 1. Performance with different objectives.

	4x	100x	40x+mass
Mass	47.8 g	88.8 g	163.3 g
Resonance Freq.	412 Hz	378 Hz	264 Hz
Force Feedback BW.	500 Hz	398 Hz	326 Hz
Tracking BW. (PID)	31.6 Hz	26.1 Hz	21.5 Hz
Tracking BW. (OIFF+S. PI)	167 Hz	255 Hz	212 Hz

5.2 Tracking Control

The performance of the commercial PID controller was tuned experimentally as there was no direct access to the PID parameters on the commercial controller. The tuning minimized the settling time due to a step input reference. The implemented PID controller has the following structure

$$C_t(s) = k_p + \frac{k_i}{s} + \frac{k_d s}{\tau_d s + 1}. \quad (21)$$

where $k_p = 0.01$, $k_i = 2000$, $k_d = 1 \times 10^{-6}$ and $\tau_d = 1.25 \times 10^{-7}$. The derivative component is an approximation that facilitates practical implementation. The approximation acts as a derivative at low frequency, while reducing the gain at high frequency with an additional pole. The term τ_d limits the gain, hence, the high-frequency signal is amplified at most by a factor of $k_d/\tau_d = 8$.

The proposed tracking control with Structure PI is

$$C_t(s) = \frac{700(s + 2914)}{2914s} \quad (22)$$

where $s = -2914$ is the additional pole. The only tuning parameter here is K_t which was tuned to provide acceptable stability margins. The closed-loop frequency responses are shown in Fig. 14 for different objectives. The performance results are summarised in Table 1. The performance of the proposed control scheme shows a significant improvement as compared to the commercial PID controller.

6. CONCLUSION

This paper describes a novel method of increasing the tracking bandwidth of an objective lens positioner used in confocal microscopes. The objective lens positioner is first damped using a damping controller technique called Optimal Integral Force Feedback which enables the mechanical damping of the system to be increased arbitrarily through the additional of a feed-through term which changes the zeros location of the system. The experimental results on the objective lens positioner demonstrate an increase in the maximum damping from 0.33 to 0.68. Furthermore, we show that with different objective lenses, the system is still damped effectively. We proceed to design a Structured PI tracking controller. This eliminates an additional real pole induced by OIFF which limits the bandwidth of traditional integral tracking controllers. The performance of the proposed method is compared to a commercial PID controller. With the proposed controllers, the tracking bandwidth of the system is increased from 26.1 Hz to 255 Hz, an improvement of almost ten folds.

REFERENCES

D. Y. Abramovitch, S. Hoen, and R. Workman. Semi-automatic tuning of PID gains for atomic force micro-

- scopes. In *Proc. American Control Conference*, pages 2684–2689, Seattle, WA, June 2008.
- S. S. Aphale, A. J. Fleming, and S. O. R. Moheimani. Integral resonant control of collocated smart structures. *IOP Smart materials and Structures*, 16:439–446, April 2007.
- S. S. Aphale, B. Bhikkaji, and S. O. R. Moheimani. Minimizing scanning errors in piezoelectric stack-actuated nanopositioning platforms. *IEEE Transactions on Nanotechnology*, 7(1):79–90, January 2008.
- S. Devasia, E. Eleftheriou, and S. O. R. Moheimani. A survey of control issues in nanopositioning. *IEEE Transactions on Control Systems Technology*, 15(5):802–823, September 2007.
- A. A. Eijsen, M. Burger, J. T. Gravdahl, and K. Y. Pettersen. PI²-controller applied to a piezoelectric nanopositioner using conditional integrators and optimal tuning. In *Proc. IFAC World Congress*, volume 18, Milano, August 2011. doi: 10.3182/20110828-6-IT-1002.01401.
- J. L. Fanson and T. K. Caughey. Positive position feedback control for large space structures. *AIAA Journal*, 28(4):717–724, 1990.
- A. J. Fleming. Nanopositioning system with force feedback for high-performance tracking and vibration control. *IEEE Transactions on Mechatronics*, 15(3):433–447, June 2010.
- A. J. Fleming and K. K. Leang. Integrated strain and force feedback for high performance control of piezoelectric actuators. *Sensors and Actuators A*, 161(1-2):256–265, June 2010. doi: 10.1016/j.sna.2010.04.008.
- A. J. Fleming and K. K. Leang. *Design, Modeling and Control of Nanopositioning Systems*. Springer, London, UK, 2014.
- A. J. Fleming and S. O. R. Moheimani. Sensorless vibration suppression and scan compensation for piezoelectric tube nanopositioners. *IEEE Transactions on Control Systems Technology*, 14(1):33–44, January 2006.
- A. J. Fleming, S. Behrens, and S. O. R. Moheimani. Optimization and implementation of multi-mode piezoelectric shunt damping systems. *IEEE/ASME Transactions on Mechatronics*, 7(1):87–94, March 2002.
- A. J. Fleming, S. S. Aphale, and S. O. R. Moheimani. A new method for robust damping and tracking control of scanning probe microscope positioning stages. *IEEE Transactions on Nanotechnology*, 9(4):438–448, September 2010. doi: 10.1109/TNANO.2009.2032418.
- S. Nima Mahmoodi and Mehdi Ahmadian. Modified acceleration feedback for active vibration control of aerospace structures. *Smart Materials and Structures*, 19(6):065015, 2010.
- Rachel A Oliver. Advances in afm for the electrical characterization of semiconductors. *Reports on Progress in Physics*, 71(7):076501, 2008.
- H. R. Pota, S. O. R. Moheimani, and M. Smith. Resonant controllers for smart structures. In *Proc. IEEE Conference on Decision and Control*, pages 631–636, Phoenix, Arizona, December 1999.
- William H Press, Saul A Teukolsky, William T Vetterling, and Brian P Flannery. *Numerical recipes 3rd edition: The art of scientific computing*. Cambridge university press, 2007.
- A. Preumont. *Vibration control of active structures*. Kluwer Academic Publishers, 2002.
- A. Preumont. *Mechatronics, Dynamics of electromechanical and piezoelectric systems*. Springer, Dordrecht, The Netherlands, 2006.
- A. Preumont, J. P. Dufour, and C. Malekian. Active damping by a local force feedback with piezoelectric actuators. *AIAA Journal of Guidance and Control*, 15(2), 1992.
- A. Preumont, B. de Marneffe, A. Deraemaeker, and F. Bossens. The damping of a truss structure with a piezoelectric transducer. *Computers and Structures*, 86, 2008.
- S. M. Salapaka and M. V. Salapaka. Scanning probe microscopy. *IEEE Control Systems*, 28(2):65–83, April 2008.
- Denis Semwogerere and Eric R Weeks. Confocal microscopy. *Encyclopedia of Biomaterials and Biomedical Engineering*. G. Wnek, and G. Bowlin, editors. Taylor and Francis, New York, 2005.